Combustion and Flame 159 (2012) 3448–3453

Contents lists available at SciVerse ScienceDirect

Combustion and Flame

journal homepage: www.elsevier.com/locate/combustflame

# Effect of oxide shell growth on nano-aluminum thermite propagation rates

Jeffrey Gesner [a], Michelle L. Pantoya [a,*], Valery I. Levitas [b,c,d]

[a] Texas Tech University, Department of Mechanical Engineering, Lubbock, TX 79409, United States
[b] Iowa State University, Department of Aerospace Engineering, Ames, IA, United States
[c] Iowa State University, Department of Mechanical Engineering, Ames, IA, United States
[d] Iowa State University, Department of Material Science and Engineering, Ames, IA, United States

ARTICLE INFO

*Article history:*
Received 9 April 2012
Received in revised form 6 June 2012
Accepted 6 June 2012
Available online 28 June 2012

*Keywords:*
Aluminum oxidation
Nanoparticles
Flame speeds
Thermite combustion

ABSTRACT

Flame propagation rates for nanometric particle composites of aluminum (Al) and molybdenum trioxide ($MoO_3$) were examined. The Al particles were prepared by thermally treating the particles at 480 °C for time increments up to 180 min in oxygen and 90 min in argon. This treatment caused the aluminum passivation shell to grow and there is also evidence of shell damage due to treatment. Results reveal several interesting behaviors: flame speeds initially on the order of several hundred meters per second were reduced with damage to the oxide shell, and there is a weak dependence of the flame speed on the ratio of particle radius to shell thickness ($M$) in the range $6.1 < M < 13.4$. The sharp drop in flame rate at further reduction in $M$ down to 5.0 is consistent with a similar drop observed for adding alumina to the reactive mixture. All observations are consistent with the melt dispersion mechanism associated with Al nanoparticle oxidation.



## 1. Introduction

Thermites are composite energetic materials and are described here as consisting of a metallic fuel (i.e., aluminum, Al) combined with a solid oxidizer (i.e., molybdenum trioxide, $MoO_3$) [1]. These formulations have been historically valued for their ability to produce high heats of reaction and combustion temperatures [2]. Recent development in processing techniques have allowed for the production of fuel and oxidizer particles in the nano-scale regime. Aluminum based thermites have been shown to have greatly increased reaction rates when particle size is reduced to the nanometer scale [3–7]. Some publications report decreased activation energy [4,6,8,9] and others found decreased aluminum melting temperature [10–12]. However, the reduction in melting temperature does not exceed 10 K for particles with diameter greater than 40 nm, while the maximum possible flame rate of about 1000 m/s is observed for particles up to 120 nm in diameter [13]. Detailed analysis of the validity of such an extrapolation is given in [14]. Several researchers have proposed advanced diffusion-based models describing nano-Al particle oxidation.

One model proposed by Zachariah and coworkers is based on modification of the diffusion coefficients for metal and oxygen across an oxide shell nanoparticle through introduction of a convective force driven by pressure gradient [15]. Another approach taken by Dreizin and coworkers describes oxidation in terms of a series of polymorphic phase transitions within the alumina shell [10,16–18]. The model emphasizes the thickness dependent multiple phase transitions in alumina during particle heating and predicts complex heating and oxidation kinetics. This model was derived for relatively slow oxidation rates and with experiments involving micron scale particles such that nanoparticle behavior could be extrapolated [10,16].

A third model proposed by Levitas et al. is based on a mechanochemistry approach and is applicable only at high heating rates [13,14,19,20]. The theory describes heating, phase change and rapid pressure buildup within the fuel particle core. The mechanism has been coined the melt dispersion mechanism because it results in a burst-like dispersion of molten fuel [19]. More specifically, melting of the Al core is accompanied by a 6% increase in volume which places the oxide shell under tremendous hoop stress. The shell eventually fails and dynamic spallation occurs. After this, the unbalanced pressure causes an unloading wave propagating to the particle center which generates large tensile pressure and disperses small molten aluminum clusters into the reaction zone to be readily oxidized. In this theory, the key controlling parameter is not the shell thickness or particle size, but the ratio between the two. This ratio is denoted as $M$, where $R$ is the Al core radius, $\delta$ is the shell thickness, and $M = R/\delta$.

A significant implication of this theory is that the propagation rate will increase with increasing oxide shell thickness, up to a certain critical value: $M_{crit} = 19$ [13]. This theory suggests a different approach to processing aluminum powders in which micron particles could potentially perform as well as their nanoscale coun-

* Corresponding author.
*E-mail address:* michelle.pantoya@ttu.edu (M.L. Pantoya).

0010-2180/$ - see front matter © 2012 The Combustion Institute. Published by Elsevier Inc. All rights reserved.
http://dx.doi.org/10.1016/j.combustflame.2012.06.002

terparts as long as the particles could be made to melt and disperse.

In a recent study [21], an increase in particle reactivity was demonstrated when the alumina shell is pre-compressed and the Al core is pre-expanded. Pre-stressing was produced by heating particles to several elevated temperatures, holding them at a temperature for 10 min to relax thermal stresses, and cooling them at several rates to room temperature. For the heating to 105 °C and cooling at 0.13 °C/s, flame propagation speed increased by 31% for nanoparticles and for 41% for micron particles. These results were quantitatively consistent with the theoretical predictions based on the melt-dispersion mechanism.

The objective of this study is to examine the propagation rates of Al + $MoO_3$ by synthesizing Al particles with controlled and varied oxide shell thicknesses and thus varying *M*. The synthesis approach is to thermally treat Al particles at temperatures as high as 480 °C for up to 180 min in a pure oxygen environment and monitor the particle shell thickness using transmission electron microscope (TEM). Such a treatment changes not only oxide thickness but also creates significant internal stresses during and after cooling, leading to defective shell. Flame propagation rates are measured from high speed video data of powders propagating in a semi-confined tube apparatus; a benchmark diagnostic for comparing thermite formulations [5,22,23].

## 2. Experimental

The experimental approach involved heat treating Al particles in an isothermal furnace to control alumina passivation shell growth. Particles were characterized using a thermogravimetric analyzer (TGA) and TEM. Flame propagation was analyzed using semi-confined flame tubes. Each phase of this study will be described in more detail here.

### 2.1. Materials

A summary of Al particles prepared in this study is presented in Table 1. Aluminum powder was supplied by Sigma Aldrich with an average particle size of 95 nm and a nominal purity of 99.5%. These particles were treated in a 480 °C isothermal environment for up to 180 min. The notation Al-0 m corresponds to untreated Al as received by the supplier and Al-30 m denotes Al particles treated at 480 °C for 30 min. The reported active content for the Al-0 m aluminum was calculated from the measured shell thickness. Molybdenum trioxide ($MoO_3$) was supplied by Nanostructured & Amorphous Materials, Inc. and combined with Al particles for the flame propagation rate studies. The $MoO_3$ particles have an average particle size of 370 nm.

### 2.2. Thermogravimetric analysis

A baseline analysis of Al oxidation was performed using a Netzsch STA 409 PC Luxx thermogravimetric analyzer (TGA). The TGA is capable of measuring mass with a precision of 0.001 mg and thus monitors the weight gain as Al is oxidized to alumina. For this analysis, 11.48 mg of untreated Al was held in a platinum crucible in a controlled environment of ultra-high purity oxygen. Pure oxygen was chosen over atmospheric air to prevent any possible reactions with nitrogen or humidity, as aluminum has been shown to form nitrides [24]. The chamber was then heated at a rate of 40 °C per minute until the isothermal temperature of 480 °C was reached. The isotherm was held for 180 min and mass gain monitored.

### 2.3. Growing the oxide shell

The data produced in the TGA analysis provided mass gain and oxidation information to enable larger Al sample sizes to be heat treated in an isothermal furnace by controlling duration of heat treatment. A Neytech Qex oven was used for this purpose. A programmable interface allowed for automated control of ramp rate, isotherm time, and purge gas flow, producing consistent and accurate heating profiles. Six samples of Al powder were prepared by oxidation in a pure oxygen environment at 480 °C for different lengths of time varying up to 150 min. The isotherm temperature of 480 °C was chosen because this temperature provided reasonable reactions rates based on several TGA/DSC trial runs that indicated 480 °C is high enough to allow oxidation and shell growth to be completed within several hours.

For each heat treatment, roughly 900 mg of Al powder were prepared. The oven chamber was purged with ultra-high purity oxygen flowing 180 cc/min for a period of 10 min. This allowed for the volume to be flushed five times with the purge gas, giving a statistical purity of 99% oxygen in the chamber. The temperature was ramped at a rate of 200 °C/min until the isotherm temperature of 480 °C was reached. The temperature was then held constant for different lengths of time, producing Al samples with varying oxide shell thicknesses.

### 2.4. Transmission electron microscopy

A Jeol JEM-2100 high resolution transmission electron microscope (TEM) was used to image the Al particles at 200 kV. This thermoionic emission microscope used a LaB6 filament. The particles were dispersed in methanol solution and positioned onto a copper disk with carbon webbing. Several particles from each aluminum batch were imaged. Gatan image analysis software was used to measure the oxide shell in three different places for each particle. These values were averaged to give a mean shell thickness. Additionally, roughly 100 particle diameters were measured at lower magnifications giving an average particle diameter of 95 nm. This value was close to the statistical median and mode in the size distribution plot.

### 2.5. Thermite preparation

Thermites were prepared with a constant equivalence ratio of $\Phi = 1.3$ and thus with varying alumina content. Mixtures were

**Table 1**
Aluminum powder properties.

| Material | Diameter (nm) | Isotherm time (min) | Shell thickness (nm) | % Active | *M* value |
|---|---|---|---|---|---|
| Al-0 m | 95 | 0 | 2.7 | 88.3 | 16.7 |
| Al-8 m | 95 | 8 | 3.3 | 86.5 | 13.4 |
| AM-15 m | 95 | 15 | 4.5 | 84.4 | 9.6 |
| Al-30 m | 95 | 30 | 4.6 | 79.8 | 9.3 |
| Al-60 m | 95 | 60 | 5.7 | 75.5 | 7.3 |
| Al-90 m | 95 | 90 | 6.7 | 74.1 | 6.1 |
| AM-150 m | 95 | 150 | 8.3 | 67.3 | 5.2 |
| $MoO_3$ | 370 | x | x | 99.5 | x |

prepared using a previously well described sonification process and produce a homogeneous mixture [25].

### 2.6. Flame propagation experiments

Figure 1 is a schematic of the flame propagation rate experiments. The thermite was carefully loaded into the steel tube until the powder was flush with the opening. The tube was lightly tapped to reduce density gradients and eliminate air pockets, and then additional powder was loaded into the tube. The tube was weighed before and after powder loading to provide data for charge density. Charge density was fairly consistent around 0.40 g/cc. The tube was secured to a fixture inside a steel blast chamber with an acrylic window. The ignition system provided current to the filament while simultaneously triggering the camera.

A Vision Research Phantom v7.1 high speed camera was used to take high speed video of the combustion event. Video was recorded at 47,000 frames per second at an exposure of 16 μs. The phantom software was used to track the position of the flame front with respect to time. The forward-most saturated pixel was defined as the front of flame propagation. A line was fit through the last four points on each position versus time trace and the slope corresponds with the flame propagation rate.

### 2.7. Thermal equilibrium modeling

The Al–$MoO_3$ reaction was modeled as a constant volume explosion using thermal equilibrium software, Cheetah [26]. The proportion of alumina in the mixture was incrementally increased while keeping the ratio of aluminum to molybdenum trioxide constant at $\Phi = 1.3$. An initial density of 0.40 g/cc was chosen as this was a typical density for a loaded tube shot. This analysis enabled a correlation between combustion properties theoretically predicted and the experimental measurements as a function of alumina content.

## 3. Results and discussion

### 3.1. Mass gain

Figure 2 shows Al mass gain over an extended duration at 480 °C in a pure oxygen environment. The smooth curve is data taken from the TGA, while the points represent mass gain from the oven heat-treated Al samples. All mass gain is assumed to be from the addition of oxygen which reacts with Al to form alumina, as given in the equation:

$$3Al + O_2 \rightarrow Al_2O_3.$$

The oven treated Al particles do not align precisely with the TGA data and reflect slightly more mass gain that anticipated from the TGA data. In the TGA, the platinum crucible was covered with a lid containing a pinhole for gas to escape. It is possible that this pinhole was small enough to bottleneck the mass transport of oxygen into the crucible, limiting the oxidation rate. The crucible in the oven was uncovered and therefore would not experience the same constraint. Additionally, while the oven was ramped at a rate of 200 °C/min the TGA was ramped at only 40 °C/min. This difference in heating rate may also have an effect on oxidation behavior, in particular, through higher thermal stresses and some damage to the oxide shell for higher heating rate, when stresses have shorter time to relax.

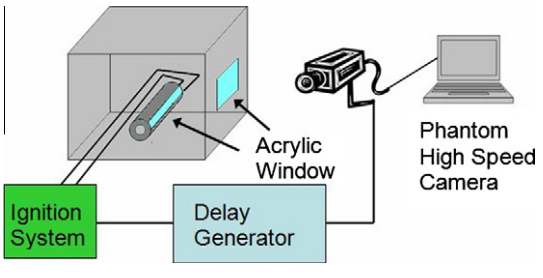


**Fig. 1.** Experimental setup representing the flame speed measurements.

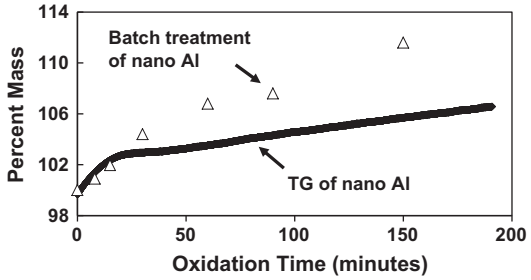


**Fig. 2.** Aluminum mass gain during thermogravimetic (TG) analysis (solid line) and in treated batches (open triangle symbol).

### 3.2. Shell growth

Figure 3 shows the TEM micrographs of an untreated and heat-treated Al particle, respectively. The treated particle was held in a pure oxygen environment at 480 °C for 90 min. The images show that the oxide shell has grown significantly. The white fringes along the outside of the particle are an optical artifact from interference and are not included in the shell thickness or diameter measurements. Several particles from each batch were imaged, and for each particle the shell was measured three times. Measurements were taken only of particles that were not overlapping. These values were then averaged together. The average shell thicknesses are reported in Fig. 4. Lower magnification images were taken of clusters of particles. The diameters of roughly 100 of these particles were then measured and these values were averaged together. This produced an average (mean) diameter of 95 nm for the aluminum powder. While there was a large size distribution in among the particles (standard deviation of 45 nm), this was the case for all our previous studies, and operating with averaged size and $M$ proved to be reasonable.

It can be seen that the oxidation rate decreases with time after 15 min. As the oxide shell grows, it presents a barrier to the diffusion of aluminum cations, thus limiting the oxidation rate and growth rate of the shell.

The thickness of the oxide layer can be estimated using Eq. (1) given the percent aluminum content and densities of the metal and metal oxide.

$$\frac{R^3}{(R-\delta)^3} = \frac{\rho_m}{\rho_{mo}}\left(\frac{1}{1/Y^{-1}}\right) + 1 \tag{1}$$

In Eq. (1) $R$ is the radius of the spherical particle, $\delta$ is the thickness of the oxide layer, $\rho$ is the density of the metal ($m$) or metal oxide ($mo$), and $Y$ is the mass fraction of metal oxide to total particle mass, as derived from the active content. The oxide shell was measured on the untreated aluminum to be 2.7 nm. Using the equation above, and assuming a diameter of 95 nm, it can be calculated that the untreated powder was an average of 88.3% pure aluminum. This initial aluminum content was then used to estimate the shell thicknesses for a given mass gain. These estimates along with the measured shell thickness are reported in Fig 4.

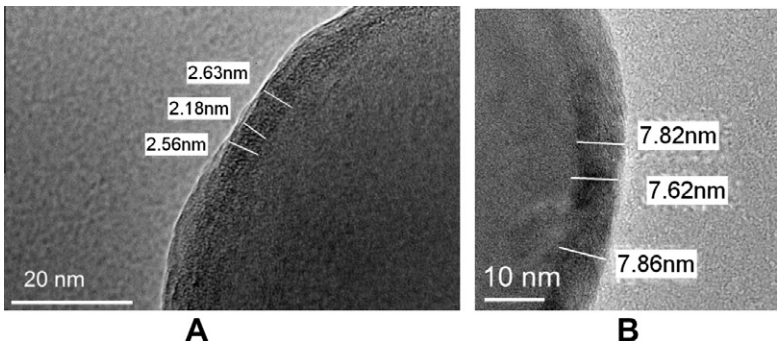


**Fig. 3.** TEM micrograph of oxide shells on (A) Al-0 m and (B) Al-90 m.

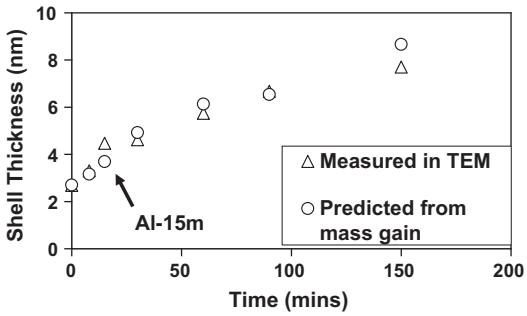


**Fig. 4.** Measured oxide shell thickness for treated aluminum with predicted shell thickness as expected from mass gain. Triangles indicate measured thicknesses, while circles indicate calculated thicknesses.

While the Al-15 m batch has a weight gain in line with the other data (see Fig. 2), the shell thickness is unexpectedly large. Re-imaging this batch of particles in the TEM confirmed the original shell thickness measurement.

It has been reported [16,27] that the oxide shell undergoes a phase transition from an amorphous to a crystalline structure during the growth process. In the temperature range used, the $\gamma$-$Al_2O_3$ phase of alumina is thermodynamically favorable. However, due to surface interactions with the aluminum, the $Al_2O_3$ exists in the amorphous phase until a critical thickness of roughly 4 nm is reached. At this point the oxide transitions to the $\gamma$-$Al_2O_3$ phase which has a lower specific volume than the amorphous phase [16]. This may or may not potentially lead to a cracked shell, depending on whether change in volume occurs isotropically or just reduces the shell thickness without causing significant hoop stresses [14].

If the shell does crack, the cracks provide a channel of least resistance for the diffusion of aluminum and oxygen ions, leading these areas to oxidize more quickly than those covered with a thick shell. In this way, the cracks fill in with alumina and then undergo a "healing" process.

The Al-15 m particles were the first batch to transition past this critical thickness of 4 nm. The batches treated beyond this point would have had time for the shell to heal in the oven, which, presumably, would be relatively quick in the hot, oxygenated environment. The Al-15 m batch, however, was taken out of the oven shortly after the phase transition. Also, the shell after 15 min was relatively thin, and the total stresses therefore are higher than for a larger shell, leading to more intense damage.

Additionally, cooling down to the room temperature generates large internal stresses, which lead to cracking of the shell and possible delamination of the shell from the core. In the case of delamination, it may even lead to ignition during the cooling, as it was reported for micron particles in [28]. In our case, while ignition was not observed, a significant weight gain after heat treatment in the Al-15 m batch would suggest significant distributed cracking of the oxide shell. It is possible that when this batch was weighed, the shell was cracked in the healing process and continued to react with the ambient environment after being weighed. This would explain why the shell growth is beyond what would be expected from the measured mass gain.

To investigate the thermal effects of the heating profile on the oxide shell, a batch of aluminum was treated with the same gas flow rate and heating profile as the Al-90 m, but with argon flowing into the chamber instead of oxygen. Surprisingly, the argon treated particles significantly gained weight and increased oxide shell thickness up to 8 nm, similar to oxygen treated particles. Since they could not oxidize while being in argon atmosphere, this indicates that oxidation occurred after removing particles from the oven. This can be explained as follows. Keeping particles in the oven at 480 °C without reaction leads to relaxation of internal stresses as the temperature changes and the particle is stress-free to 480 °C. Such a treatment is similar to that in [21] but at much higher temperature. Then cooling down to the room temperature generates large internal stresses, which lead to cracking of the shell and possible delamination of the shell from the core. In case of delamination, it may even lead to ignition during the cooling, as it was reported for micron particles in [28]. In our case, while ignition was not observed, significant weight gain after heat treatment in argon suggest distributed cracking of the oxide shell.

Similar consideration about increase in stress-free temperature $T_0$ is valid for particles oxidized in an oven or TGA. However, due to volume increase during chemical reaction, additional stresses appear which may not relax during holding at 480 °C. On the other hand, after cooling total stresses and extent of damage in oxidized particles may be smaller than in not oxidized, because oxidized particles have larger shell thickness.

Thus, damage to the oxide shell is expected for all treated particles: (a) due to thermal stresses at cooling down from 480 °C to room temperature [28]; (b) due to change in volume during reaction [28], and (c) due to phase transformation in a shell [14,15].

### 3.3. Flame propagation rates

The flame propagation rates for the treated Al are shown in Fig. 5 along with the pressure calculations from Cheetah. It can be seen that constant volume pressure predicted by Cheetah decreases as active Al content is reduced (i.e., greater presence of alumina). The alumina that is added to the system is inert and acts as a heat sink, decreasing reaction temperatures and slowing the reaction kinetics. Furthermore, each unit volume (or mass) of thermite will contain less moles of reactants. This will in turn produce less gas, and lower pressures, as reported by Cheetah. Aluminum based nanoparticle thermites, including Al + $MoO_3$, have been

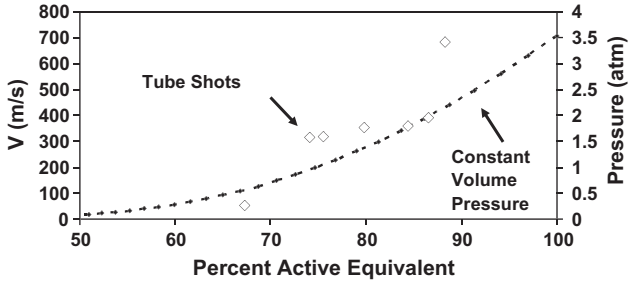


**Fig. 5.** Flame speed as a function of active aluminum content with constant volume pressure as predicted by Cheetah. Equivalence ratio of $\Phi = 1.3$.

conjectured to propagate by convective energy transfer [5,22]. With less gas produced at a lower pressure, convection may be hindered resulting in slower propagation rates. Under the assumption that the melt dispersion mechanism (MDM) is not activated at low propagation rates (i.e., <100 m/s) [19,20], the Cheetah predictions are a good indicator of thermite reactivity.

Figure 6 reports the flame speeds as a function of $M$, where the ratio $M = R/\delta$ $R$ is Al core radius and $\delta$ is alumina shell thickness). Human error in the flame speed diagnostic was found was found to be approximately 6 m/s. These error bars are smaller than the data symbols.

The maximum propagation rate is for untreated particles, 682 m/s is close to the 627 ± 19 m/s that has been previously reported for this mixture [21]. For any $M$, flame propagation speeds are well above 10 m/s, which is too high for diffusion mechanism but provides required heating rates for activation of melt dispersion mechanism [29]. Any treatment of particles leading to $6.1 < M < 13.4$ reduced flame rate down to $315 \pm 6 < V < 392 \pm 6$ m/s, which is consistent with the suppression effect of damage to oxide shell on melt-dispersion mechanism [29]. Doubling the shell thickness from 3.3 nm (Al-8 m) to 6.7 nm (Al-90 m) only depressed the flame rate about 20% (from 392 m/s to 317 m/s, respectively). The fact that the flame rate is almost constant in the range $6.1 < M < 13.4$ also consistent with predictions based on melt dispersion [19].

Note that the actual prediction based on melt dispersion mechanism is that with decreasing $M$, flame rate reaches its maximum when the entire melt is dispersed and participates in reaction, and cannot grow further because there is nothing to improve anymore. At the same time, reduction in flame rate after reaching maximum does not contradict the melt dispersion mechanism. By decreasing $M$, active aluminum content, gas generation, and consequently pressure are reduced (as reported by Cheetah, Fig. 5), which may suppress convective mechanism of flame propagation. Also, the alumina that is added to the system is inert and acts as a heat sink, decreasing reaction temperatures and slowing the reaction kinetics. The fact that in all previous experiments with undamaged particles [13,19], flame rate does not change for $10 < M < 19$ and is at the level of 950 m/s means that the effect of reaction mechanism was much stronger than the propagation mechanism and reduced Al content and gas pressure. For damaged particles here, there is some small reduction in the flame rate in the range $6.1 < M < 13.4$.

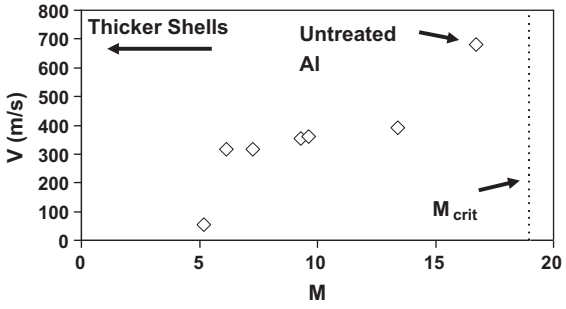


**Fig. 6.** Flame speed ($V$) as a function of $M$. The point at $M = 17$ is the untreated aluminum. $M_{crit}$ corresponds with a threshold for nanoparticles in [19,20] for maximizing the flame speed such that further decreases in $M$ will not increase the flame speed [19,20].

The shells were observed to burst in some particles after treatment. Figure 7 shows a micrograph of untreated particles (Al-0 m) on the left, with treated particles (Al-150 m) that contain an example of the burst shell. This cracking behavior has been observed previously, when particles were progressively heated past their melting point in a hot stage TEM [18,27].

In reviewing the TEM micrographs, it was observed that while the burst particles were only a small fraction of the whole, their occurrence was more prominent in the longer treated aluminum batches.

It is noted that the Al-150 m thermite did not readily ignite with the steel filament used for the other tests. More than one attempt was necessary to initiate the tube shot. When a pea-sized amount of the other mixtures were exposed to an open flame they would readily ignite with a pop. However the Al-150 m thermite was observed to react only after being exposed to an open flame for several seconds. It is interesting to note that the thermite with the slowest propagation rate was also the most difficult to ignite.

For Al-150 m Al content is around 67%, and a sharp drop in flame rate occurs down to 53 ± 6 m/s. Note that similar drop was observed for undamaged particles in [30,31] when added percentage of alumina to reactive mixture was between 15% and 20%. These numbers are close to the increase in alumina percentage due to shell growth in our experiment.

### 3.4. Unsteady propagation

Unsteady propagation has been observed when aluminum based nano-thermites are mixed to sub-optimal equivalence ratios or diluted with alumina [27,28]. Instead of a steadily accelerating flame front, these unsteady propagations are characterized by swirling, oscillating and jumping motions of the reaction front. Thermites mixed at sub-optimal equivalence can be thought of as diluted by either excess fuel or oxidizer. In a similar way, as thermites are diluted with the addition of alumina in the shell, they exhibit the same unsteady propagation patterns. Figure 8 shows the position versus time plots for the untreated and heat treated Al thermites, respectively. The breaks in the $x$–$t$ plot for the Al-90 m thermite correspond to an erratic, jumping flame front.

## 4. Conclusions

Nano aluminum particles were synthesized with different oxide shell thicknesses, producing batches of aluminum with a range of $M$ values. The chosen heat treatment at 480 °C damages alumina shell due to several possible reasons: (a) due to thermal stresses at cooling down from 480 °C to room temperature; (b) due to change in volume during reaction, and (c) due to phase transformation in a shell. This damage reduces flame speed. Flame speed of several hundred meters per second, reduction in flame rate with damage to oxide shell, and weak dependence of the flame speed on $M$ in the range $6.1 < M < 13.4$ is consistent with the melt dispersion mechanism of reaction of Al nanoparticles. When percentage of alumina exceeds a threshold of about 30% ± ~3%, flame rate sharply drops, which is consistent with results from Foley et al. [31].

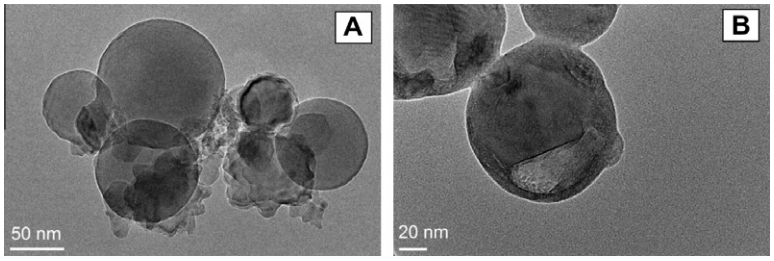


**Fig. 7.** TEM images of Al particles. (A) Al-0 m; and (B) Al-150 m.

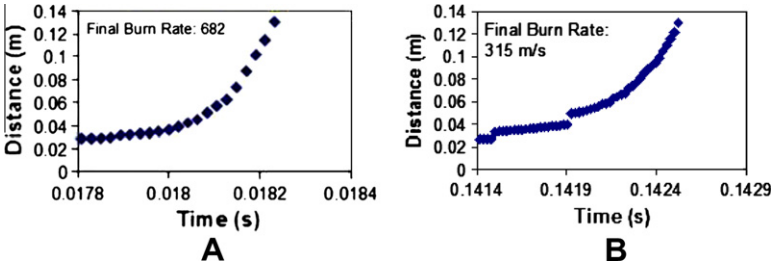


**Fig. 8.** Position versus time traces of the flame front. (A) Untreated aluminum. (B) Al-90 m.

This gave rise to unsteady, jumping flame fronts, as previously observed when bulk alumina was added to the system.

In future experiments, to avoid or reduce damage to oxide shell, temperature for treatment will be reduced. Alternatively, while keeping this temperature for oxidation to provide relatively fast kinetics, cooling down will be performed much slower, to relax stresses. It can be done down to the chosen temperature $T_0$ (temperature at which particle is stress-free), followed by fast cooling down to room temperature, in order to create pre-stressing similar to that done previously [21].

Future work could include XRD of aluminum batches to confirm crystal structure and to measure evolution of internal stresses. Also, measuring weight continuously over the course of hours/ days/ will allow us to quantitatively analyze reaction progress of the damaged particles. Starting with larger (micron) scale particles would expand the *M* value range that can be investigated.

## Acknowledgments

The authors M. Pantoya and J. Gesner are grateful for support from the Army Research Office contract number W911NF-11-1-0439 and encouragement from our program manager, Dr. Ralph Anthenien. V. Levitas and M. Pantoya acknowledge support from NSF (CBET-0755236) Special thanks to Mr. Archis Marathe for TEM imaging and Mr. Corey Farley for TGA assistance.

## References

[1] L.L. Wang, Z.a. Munir, Y. Maximov, J. Mater. Sci. 28 (1993) 3693–3708.
[2] S. Fischer, M.C. Grubelich, Theoretical energy release of thermites, intermetallics and combustible metals, in: 24th International Pyrotechnics Seminar Conf-9807, 1998.
[3] J. Sun, M.L. Pantoya, S.L. Simon, Thermochim. Acta 444 (2006) 117–127.
[4] K. Park, D. Lee, A. Rai, D. Mukherjee, M.R. Zachariah, J. Phys. Chem. 109 (2005) 7290–7299.
[5] M.R. Weismiller, J.Y. Malchi, J.G. Lee, R.A. Yetter, T.J. Foley, Proc. Combust. Inst. 33 (2) (2011) 1989–1996.
[6] A. Pivkina, Y. Frolov, D. Ivanov, Combust. Explos. Shock Waves 43 (1) (2007) 51–55.
[7] J.A. Puszynski, J. Therm. Anal. Calorim. 96 (3) (2009) 677–685.
[8] C.E. Aumann, G.L. Skofronick, J.A. Martin, J. Vac. Sci. Technol., B 13 (3) (1995) 1178–1183.
[9] E.M. Hunt, M.L. Pantoya, J. Appl. Phys. 98 (3) (2005) 034909.
[10] M.A. Trunov, S.M. Umbrajkar, M. Schoenitz, J.T. Mang, E.L. Dreizin, J. Phys. Chem. B 110 (26) (2006) 13094–13099.
[11] J. Eckert, J. Holzer, C. Ahn, Z. Fu, Nanostruct. Mater. 2 (1992) 407–413.
[12] J. Sun, S.L. Simon, Thermochim. Acta 463 (2007) 32–40.
[13] A. Rai, K. Park, L. Zhou, M.R. Zachariah, Combust. Theor. Model. 10 (5) (2006) 843–859.
[14] M. Trunov, M. Schoenitz, X. Zhu, E. Dreizin, Combust. Flame 140 (4) (2005) 310–318.
[15] M.A. Trunov, M. Schoenitz, E.L. Dreizin, Combust. Theor. Modell. 10 (4) (2006) 603–623.
[16] A. Rai, D. Lee, K. Park, M.R. Zachariah, J. Phys. Chem. 108 (39) (2004) 14793–14795.
[17] V.I. Levitas, M.L. Pantoya, B. Dikici, Appl. Phys. Lett. 92 (1) (2008) 011921.
[18] K.W. Watson, M.L. Pantoya, V.I. Levitas, Combust. Flame 155 (4) (2008) 619–634.
[19] V.I. Levitas, B.W. Asay, S.F. Son, M. Pantoya, J. Appl. Phys. 101 (8) (2007) 083524.
[20] V.I. Levitas, B.W. Asay, S.F. Son, M. Pantoya, Appl. Phys. Lett. 89 (71909) (2006) 1–4.
[21] V.I. Levitas, B. Dikici, M.L. Pantoya, Combust. Flame 158 (7) (2011) 1413–1417.
[22] M.R. Weismiller, J.Y. Malchi, R.A. Yetter, T.J. Foley, Proc. Combust. Inst. 32 (2) (2009) 1895–1903.
[23] B. Dikici, M.L. Pantoya, V. Levitas, Combust. Flame 157 (8) (2010) 1581–1585.
[24] A. Gromov, V. Vereshchagin, J. Eur. Ceram. Soc. 24 (2004) 2879–2884.
[25] E.L. Dreizin, Prog. Energy Combust. Sci. 35 (2) (2009) 141–167.
[26] K. Glaesemann, L.E. Fried, Recent advances in modeling hugoniots with Cheetah, in: Shock Compression of Condensed Matter, 2006, pp. 1503–1506.
[27] D.A. Firmansyah et al., J. Phys. Chem. 116 (2012) 404–411.
[28] V. Rosenband, Combust. Flame 137 (2004) 366–375.
[29] M.L. Pantoya, V.I. Levitas, J.J. Granier, J.B. Henderson, J. Propul. Power 25 (2) (Mar. 2009) 465–470.
[30] J. Malchi, R. Yetter, T. Foley, S. Son, Combust. Sci. Technol. 180 (2008) 1278–1294.
[31] T.J. Foley, A.N. Pacheco, V.E. Sanders, S.F. Son, B.W. Asay, The effect of added alumina on the propagation behavior of the nanoaluminum and molybdenum (VI) oxide system, 13th Int. Det. Symp., 2006, pp. 1217–1228.